CHARACTERIZING LUNAR IMPACT-RELATED FEATURES, EMPLACEMENT AND DEGRADATION PROCESSES: IMPACT MELTS AT COPERNICUS CRATER

M.A. Matiella Novak[1], G. W. Patterson [1], B. T Greenhagen[1], C. Neish[2], R. Smith[3] [1]Johns Hopkins University Applied Physics Laboratory, 11101 Johns Hopkins Road, Laurel, MD 20723, [2]University of Western Ontario, London, ON, [3]South River High School, Edgewater, MD. Corresponding Author: alexandra.matiella.novak@jhuapl.edu

Introduction:

- **Many questions remain about how well we can characterize the processes that lead to emplacement and degradation of the Moon's regolith, both at the surface and sub-surface, and how well we can correlate those processes to age. Previous work has compared Diviner rock abundance data to Mini-RF surface roughness values to investigate relationships between crater age and regolith degradation [1,2,3].**
- **Those initial studies suggested that the physical properties of crater features of different ages manifest differently depending on the wavelength region used in analysis because the data is detecting physical attributes at different scales and depths in the regolith. Here we focus on integrating Mini-RF-sourced surface roughness values, Diviner rock abundance, and Lunar Reconnaissance Orbiter Camera (LROC) boulder counting to compare the relative degradation rates of similar age features in different regolith settings, both at the surface and sub-surface (< a few meters).**
- **We compare Miniature Radio Frequency (Mini-RF) circular polarization ratio (CPR) values of impact melts associated with Copernicus Crater (9.3°N, 339.9°E) to optical boulder count and thermal-emission derived rock abundance data. We use these comparisons to analyze how the integration of this data can give us insight into surface and subsurface regolith degradation rates and processes, focusing on impact melts within different settings (impact melt ponds vs. impact melt flows).**
- **The two target features that we focus our analysis on are impact melt formations – one to the south and one to the northeast of Copernicus crater. The flow to the south is characterized as a melt pond with flow textures along the margins, and the flow to the northeast is characterized as melt within an ejecta blanket (i.e. non-pond).**

Target Selections: Recent research on crater features, such as impact ejecta, impact melt, and degradation rates [1,2,5] have been consulted for target areas that have been studied using Mini-RF and Diviner data. A new survey of impact melt flows in the Mini-RF data set provides a more complete global picture of these flow features, providing insight on fundamental questions about the emplacement of melt during the impact cratering process [5]. The table below lists crater selections for this work that were determined to be appropriate targets for this study based on previous research.

Crater	Latitude	Longitude	Diameter (km)	Age (myr)	Age ref
Aristarchus	23 .7	312.5	42 .0	132–168	Baldwin (1985)
Aristillus	33.8	1.2	55.9	1613-2063	Baldwin (1985)
Byrgius A	-24.6	296.2	18.7	48 ± 14.1	Morota et al. (2009)
Copernicus†*	9.6	339.9	99.6	773-903	Baldwin (1985)
Hesiodus E[5]	-27.9	344.6	3.0	<1100	Denevi et al. (2012)
Giordano Bruno	36.0	102.9	22.1	4 ± 1.4	Morota et al. (2009)
Humboldt	-27.0	81.0	199.5	3200-3800	Wilhelms (1987)
Langrenus	-8.9	61	132	1100-3200	Wilhelms (1987)
Theophilus†	-11.5	26.3	98.6	1100-3200	Wilhelms (1987)
Tsiolkovskiy	-20.4	129	184.4	3500 ± 100	Tyrie (1988)
Tycho	-43.3	348.8	87.0	118-162	Baldwin (1985)

*Boulder size-frequency results in this poster.
†Preliminary RA/CPR analysis in this poster.

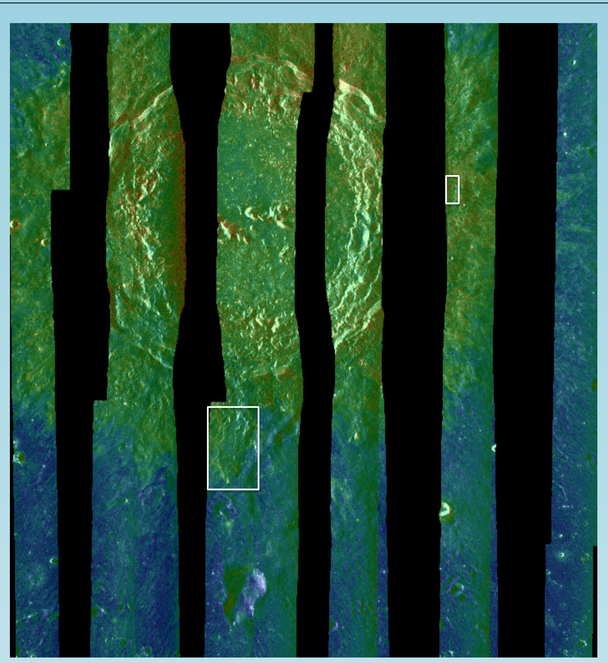

Figure 1. Mini-RF CPR . Bright greenish yellow colors correspond with greater CPR roughness values. Northeast and South regions of interest in white boxes.

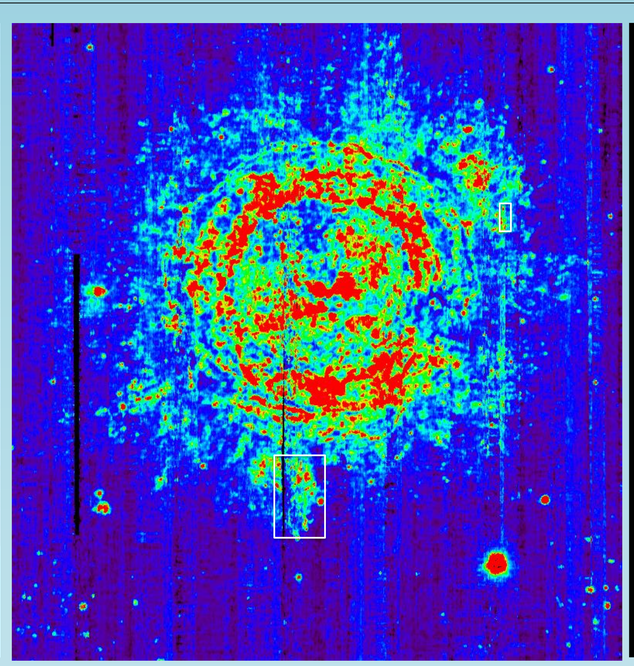

Figure 2. Diviner RA. Bright green and red colors correspond with greater rock abundance values. Northeast and South regions of interest in white boxes.

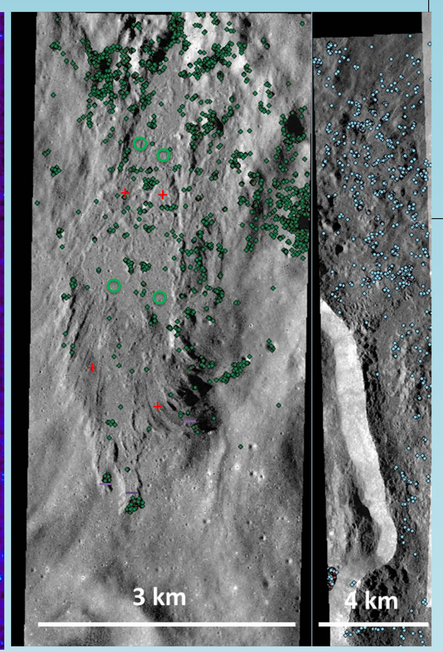

Figure 3. LRO NAC imagery with distribution of boulders >1 m diameter. Image on the left is the South melt flow and image on the right is the Northeast melt flow.

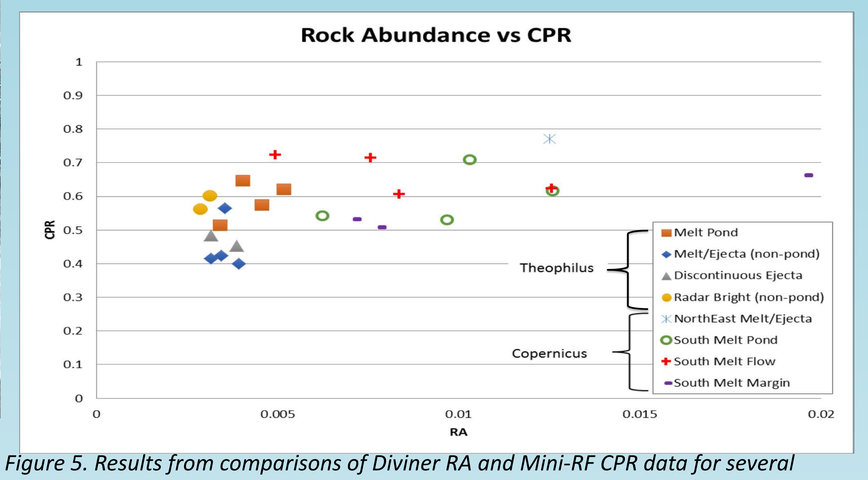

Figure 5. Results from comparisons of Diviner RA and Mini-RF CPR data for several impact-related features around Copernicus Crater, with Theophilus Crater for comparison. The Northeast melt is observed within ejecta and represents an average of values for a region of interest within the melt flow. The South melt data represents distinct points that are specific to a different unique type of feature for that flow (see Fig. 3).

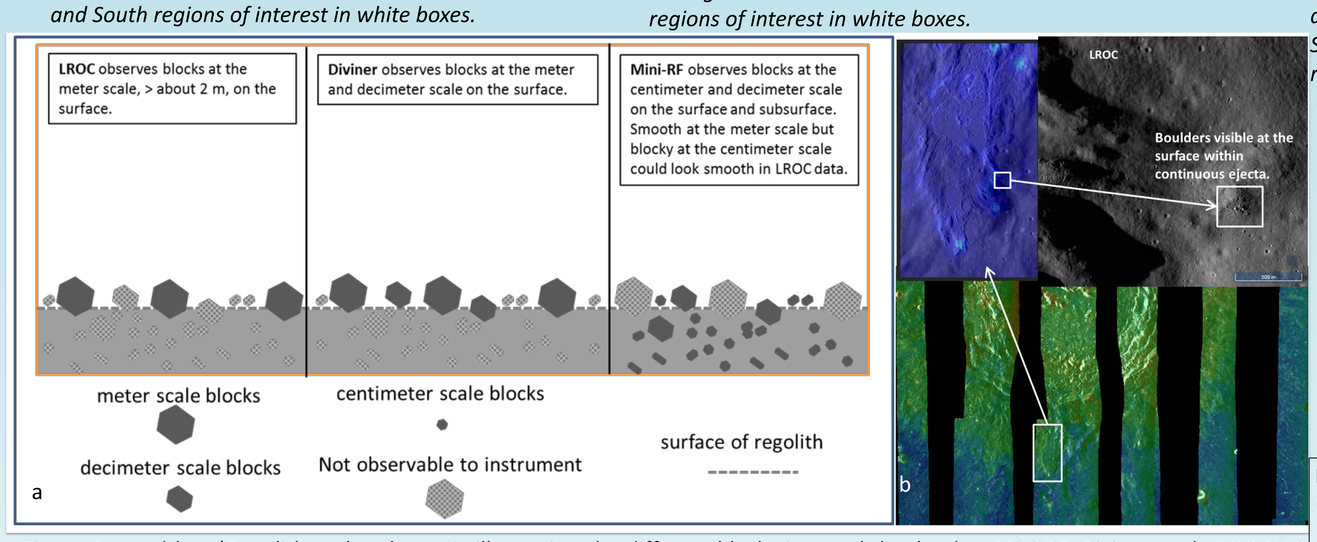

Figure 4 a and b. a.)Regolith scale schematic illustrating the different block sizes and depths that Mini-RF, Diviner, and LROC NAC observe; b.) different scales represented in data imagery.

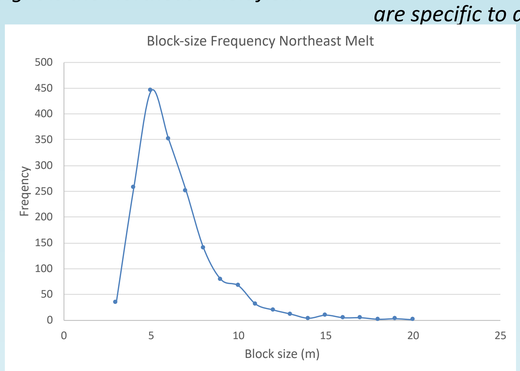

The two plots to the left and right are the result of the block-size frequency counts for the two Copernicus melts. Both show similarities among block-size frequency counts.

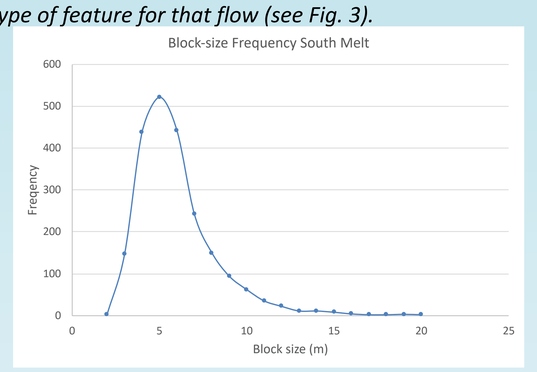

Methods: The suite of instruments onboard the NASA Lunar Reconnaissance Orbiter (LRO) are providing much needed global observations capable of better informing us on lunar surface physical properties such as surface roughness and rock abundance at both the surface and at modest depths into the regolith [3].

Diviner	Mini-RF	LROC NAC
• Diviner's rock abundance estimates leverage the wavelength dependence of thermal emission for scenes of mixed temperatures. • Bandfield and coworkers [4] produced a model for simultaneously solving for the areal fraction of rocks greater than ~0.5 to 1 m in diameter and the temperature of the rock-free regolith using thermal models and nighttime data from three of Diviner's broad thermal channels: Ch. 6 (13–23 µm), Ch. 7 (26–41 µm), and Ch. 8 (50–100 µm). • We have used global 128 pixels per degree maps of Diviner rock abundance for this analysis (Fig. 1 left).	• A hybrid polarized, side-looking, synthetic aperture radar (SAR) that primarily collected S-band (12.6 cm) observations in a monostatic "zoom" mode (15 x 30 m resolution) [3]. • Provides a unique means of analyzing the surface and subsurface physical properties of geologic deposits, including their wavelength-scale roughness, the relative depth of the deposits, and some limited compositional information. • The most common product derived and used from radar for analysis is the circular polarization ratio (CPR), which serves as a measure of surface roughness (Fig. 1 right).	• LROC Narrow-Angle Camera (NAC) observations consist of two monochrome line scan imagers with resolutions of 0.5 m/pixel. • Combined with Mini-RF and Diviner to assess the physical properties of impact features observed more readily at the surface. Additionally, we will use NAC imagery for our size-frequency boulder counting effort. • Meter-scale boulders observed in LROC data would be an accurate representation of meter-scale scatterers in CPR data (Fig. 2). • This helps constrain our observations and may produce a better means of assessing whether CPR can discriminate relative age.

Results:

1. Here we present results from an analysis at Copernicus Crater for two impact melt features south and northeast of Copernicus Crater. Both impact melt flow features are within the continuous ejecta blanket and both are associated with the formation of Copernicus Crater, and are therefore the same relative age.
2. We add this crater analysis to our previous crater study [5] and present preliminary results from integrating analysis of radar, thermal infrared and visual imaging data to physically characterize impact melt features at the surface and subsurface.
3. Figure 3 shows both impact melt features in LROC NAC data. The image on the left shows the impact melt feature to the south of Copernicus and the image on the right shows the impact melt feature to the northeast of Copernicus. The green and blue dots show the distribution of boulders >1 m diameter visible at the surface in the left and right images, respectively. Boulders visible at the surface appear to be distributed more frequently along melt margins and not as much within melt ponds.
4. Both areas also show relatively high RA values and high CPR values compared to other areas around the crater, suggesting increased surface roughness and possible sub-surface centimeter-meter scale blocks as well.
5. Although all analyzed melt features are the same age, the variability in all three data sets suggests that degradation rates are dependent on feature type. For example, flows and flow margins (i.e. non-pond) have, on average, higher values of CPR and RA, whereas pond features have generally lower values. Furthermore, despite that fact that all features fall within a similar range of CPR and RA values, only flows and flow margins contain >1m diameter boulders at the surface in LROC NAC data, whereas ponds do not. This could inform future techniques for how we use CPR and RA data to constrain ages of degradation rates of regolith formed in during crater processes.
6. We will continue integrating these data sets in order to better constrain the relative ages and degradation rates of regolith associated with various impact features and how their settings, including if they are located within mare or highlands material, factors into their degradation rates. This analysis can also inform Mini-RF planning for future targets for the currently operating bistatic campaign, and how the new Mini-RF bistatic observation mode compares to monostatic observations of the same features.

References:[1] Ghent et al. (2014) Geology, 42 (12), 1059-1062. [2] Greenhagen et al. (2016) Icarus, 273, 237-247. [3] Bandfield et al. (2011) J. Geophys. Res., 116. [4] Cahill et al. (2014) Icarus, 243, 173-190. [5] Matiella Novak et al. (2017) LPSC XLVIII, 2554